Multifrequency High-Field EPR Study of the Tryptophanyl and Tyrosyl Radical Intermediates in Wild-Type and the W191G Mutant of Cytochrome *c* Peroxidase

Anabella Ivancich,[‡] Pierre Dorlet,[‡] David B. Goodin,[§] and Sun Un*[,‡]

Section de Bioénergétique, URA 2096 CNRS, Département de Biologie Cellulaire et Moléculaire, CEA Saclay, 91191 Gif-sur-Yvette, France, and Department of Molecular Biology, The Scripps Research Institute, 10550 North Torrey Pines Road, La Jolla, California 92037.

Received October 11, 2000. Revised Manuscript Received March 14, 2001

Abstract: Multifrequency (95, 190, and 285 GHz) high-field electron paramagnetic resonance (EPR) spectroscopy has been used to characterize radical intermediates in wild-type and Trp191Gly mutant cytochrome *c* peroxidase (CcP). The high-field EPR spectra of the exchange-coupled oxoferryl−trytophanyl radical pair that constitutes the CcP compound **I** intermediate [(Fe(IV)═O) $Trp^{\bullet+}$] were analyzed using a spin Hamiltonian that incorporated a general anisotropic spin−spin interaction term. Perturbation expressions of this Hamiltonian were derived, and their limitations under high-field conditions are discussed. Using numerical solutions of the completely anisotropic Hamiltonian, its was possible to simulate accurately the experimental data from 9 to 285 GHz using a single set of spin parameters. The results are also consistent with previous 9 GHz single-crystal studies. The inherent superior resolution of high-field EPR spectroscopy permitted the unequivocal detection of a transient tyrosyl radical that was formed 60 s after the addition of 1 equiv of hydrogen peroxide to the wild-type CcP at 0 °C and disappeared after 1 h. High-field EPR was also used to characterize the radical intermediate that was generated by hydrogen peroxide addition to the W191G CcP mutant. The *g*-values of this radical ($g_x = 2.00660$, $g_y = 2.00425$, and $g_z = 2.00208$), as well as the wild-type transient tyrosyl radical, are essentially identical to those obtained from the high-field EPR spectra of the tyrosyl radical generated by γ-irradiation of crystals of tyrosine hydrochloride ($g_x = 2.00658$, $g_y = 2.00404$, and $g_z = 2.00208$). The low g_x-value indicated that all three of the tyrosyl radicals were in electropositive environments. The broadening of the g_x portion of the HF-EPR spectrum further indicated that the electrostatic environment was distributed. On the basis of these observations, possible sites for the tyrosyl radical(s) are discussed.

Introduction

Amino acid residues have proved to be relevant for enzyme catalysis as redox-active cofactors of an increasing number of metalloenzymes[1]. Tyrosyl and tryptophanyl radicals have been proposed to have a specific role in electron and proton-transfer processes in photosystem II,[2,3] ribonucleotide reductase,[4] prostaglandin H-synthase,[5,6] and DNA photolyase.[7,8] The catalytic intermediate of most heme catalases and peroxidases is believed to comprise a cationic porphyrinyl radical similar to the well-characterized compound **I** intermediates of horseradish peroxidase[9] and chloroperoxidase.[10] At variance, a tryptophanyl radical was identified as the catalytic intermediate of cytochrome *c* peroxidase.[11−14] The mechanism for the selective stabilization of the porphyrinyl or tryptophanyl radicals as the catalytic intermediates is not well-understood. From a comparative study between the active site structure of ascorbate and cytochrome *c* peroxidases, including mutations[15] and theoretical calculations,[15,16] it was proposed that the electrostatic environment and redox potentials of the porphyrin or the protein redox cofactors are responsible for the selectivity.

The catalytic site of heme catalases and peroxidases consists of an iron−protoporphyrin IX prosthetic group. The iron is pentacoordinated and in the high-spin Fe(III) oxidation state for the native enzymes. A common property of catalases and

* To whom correspondence should be addressed: Centre d'Etudes de Saclay, Section de Bioénergétique, Bat. 532, 91191 Gif-sur-Yvette, France. Tel: +33 1 69 08 28 42. Fax: +33 1 69 08 87 17. E-mail: sun@ozias.saclay.cea.fr.

‡ CEA Saclay.

§ The Scripps Research Institute.

(1) Stubbe, J.; van der Donk, W. A. *Chem. Rev.* **1998**, *98*, 705−762.
(2) Tommos, C.; Babcock, G. T. *Acc. Chem. Res.* **1998**, *31*, 18−25.
(3) Tommos, C.; Babcock, G. T. *Biochim. Biophys. Acta* **2000**, *1458*, 199−219.
(4) Gräslund, A.; Sahlin, M. *Annu. Rev. Biophys. Biomol. Struct.* **1996**, *25*, 259−286.
(5) Smith, W. L.; Eling, T. E.; Kulmacz, R. J.; Marnett, L. J.; Tsai, A. *Biochemistry* **1992**, *31*, 3−7.
(6) Shi, W.; Hoganson, C. W.; Espe, M.; Bender, C. J.; Babcock, G. T.; Palmer, G.; Kulmacz, R. J.; Tsai, A. *Biochemistry* **2000**, *39*, 4112−4121.
(7) Kim, S. T.; Heelis, P. F.; Sancar, A. *Methods Enzymol.* **1995**, *258*, 319−343.
(8) Aubert, C.; Vos, M. H.; Mathis, P.; Eker, A. P. M.; Brettel, K. *Nature* **2000**, *405*, 586−590.
(9) Schulz, C. E.; Devaney, P. W.; Wrinkler, H.; Debrunner, P. G.; Doan, N.; Chiang, R.; Rutter, R.; Hager, L. P. *FEBS Lett.* **1979**, *103*, 102−105.
(10) Rutter, R.; Hager, L. P.; Dhonau, H.; Hendrich, M.; Valentine, M.; Debrunner, P. *Biochemistry* **1984**, *23*, 6809−6816.
(11) Sivaraja, M.; Goodin, D. B.; Smith, M.; Hoffman, B. *Science* **1989**, *245*, 738−740.
(12) Mauro, J. M.; Fishel, L. A.; Hazzard, J. T.; Meyer, T. E.; Tollin, G.; Cusanovich, M. A.; Kraut, J. *Biochemistry* **1988**, *27*, 6243−6256.
(13) Erman, J. E.; Vitello, L. B.; Mauro, J. M.; Kraut, J. *Biochemistry* **1989**, *28*, 7992−7995.
(14) Hoffman, B. M. *Acc. Chem. Res.* **1991**, *24*, 164−170.
(15) Bonagura, C. A.; Sundaramoorthy, M.; Pappa, H. S.; Patterson, W. R.; Poulos, T. L. *Biochemistry* **1996**, *35*, 6107−6115.
(16) Jensen, G. M.; Bunte, S. W.; Warshel, A.; Goodin, D. B. *J. Phys. Chem. B* **1998**, *102*, 8221−8228.

10.1021/ja0036514 CCC: $20.00 © 2001 American Chemical Society
Published on Web 05/08/2001

peroxidases is the formation of the highly oxidizing intermediate, currently referred to as compound **I**,[17] which catalyzes the oxidation of various substrates (for a review, see ref 18). This intermediate originates from the two-electron oxidation of the native enzyme by hydrogen peroxide to generate the oxoferryl state (Fe(IV)═O) and the concomitant formation of a porphyrinyl ($por^{\bullet+}$) or a tryptophanyl ($Trp^{\bullet+}$) radical cation. The spectroscopic characterization of the radical species of CcP compound **I**, combined with site-directed mutagenesis studies have unequivocally identified the site of the radical formation as Trp191.[11]

The axial EPR signal observed for the compound **I** in cytochrome *c* peroxidase at 9 and 35 GHz could be modeled by a weak exchange coupling of a tryptophanyl radical and the oxoferryl moiety,[11] including a distribution in *J* values.[19,20] Such a distribution of ferro- and antiferro-magnetic interaction was also invoked to explain the very broad EPR signal of the porphyrinyl radical intermediate in horseradish peroxidase[9] and the axial EPR signal of compound **I** in *Micrococcus lysodeikticus* catalase.[21] The variation of the distribution in the exchange-coupling interaction between the tryptophanyl radical and the oxoferryl moiety has been directly correlated to the changes in the 9 GHz EPR spectrum of the compound **I** intermediate observed for the His175[22,23] and Asp235[19] mutants of cytochrome *c* peroxidase.

A limited number of heme catalase and peroxidase intermediates have been studied by EPR and ENDOR spectroscopies, two techniques that are well-suited to specifically identify the nature of the radical species formed during the catalytic cycle. Examples include catalases from *M. lysodeikticus*,[21] *Proteus mirabilis*, and bovine liver[24,25] and peroxidases such as the chloroperoxidase,[10] cytochrome *c*[11,19,20], lignin,[26] and ascorbate[15] peroxidases. For some of these enzymes, the use of the rapid-mix freeze-quench technique combined with EPR spectroscopy has allowed the detection of two different radical intermediates arising from the sequential oxidation of the porphyrin macrocycle and a protein amino acid. Specifically, tyrosyl radical intermediates have been reported for the peroxidase cycle of prostaglandin synthase[27,28] and for bovine liver catalase.[24] The EPR spectrum of amino acid-based radicals at conventional fields (0.3 T, 9 GHz) is dominated by partially resolved hyperfine couplings of the electron spin and the adjacent protons. The small *g*-anisotropy inherent to such radical species is not resolved in the 9 GHz EPR spectra. In contrast, at higher fields (95−285 GHz), it is possible to resolve the *g*-anisotropy of amino acid-based radicals. It has been demonstrated that the *g*-values are sensitive to the electrostatic environment of tyrosyl radicals.[29−32] Moreover, multifrequency EPR (9−285 GHz) has been used to better characterize the nature of the exchange coupling interaction for two $S = 1/2$ interacting systems.[33,34]

We have combined multifrequency EPR and spectral simulations to further characterize the [(Fe(IV)═O) $Trp^{\bullet+}$] intermediate of wild-type cytochrome *c* peroxidase. The tryptophanyl radical in exchange interaction with the oxoferryl moiety can be modeled by a powder-pattern spectrum with effective *g*-values that depend on the interaction parameters, the zero-field splitting (D) of the oxoferryl iron, and the *g*-values of the interacting species. The use of several frequencies (9, 95, 190 and 285 GHz) provided stricter constraints on the simulations of the EPR spectrum. Moreover, by modeling the spin coupling as an anisotropic interaction instead of as a sum of isotropic exchange terms,[19] it was possible to obtain a representation that was consistent with both the frozen-solution and the single-crystal data. We were able to clarify the issue on the narrow signal reported previously[42−44,19] for the wild-type (WT) and mutant compound **I** samples of CcP by using the greater *g*-anisotropy resolution of high-field (285 GHz) EPR and different mixing times. We have also characterized the compound **I** intermediate of the W191G mutant CcP. The multifrequency EPR spectrum of the W191G compound **I** radical showed hyperfine couplings and *g*-values that are typical of tyrosyl radicals in an electropositive environment. Possible candidates for the radical site are discussed.

Materials and Methods

Sample Preparation. The WT MKT-CcP samples were obtained from the protein expression in *Escherichia coli* by the plasmid pT7CCCP under control of the T7 promoter. CcP-MKT differs from the yeast wild type in positions 53 and 152 as well as the Met-Lys-Thr on the N-terminus.[35] The W191G mutant of CcP was constructed by site-directed mutagenesis, overexpressed in *E. coli* BL21(DE3) and purified as previously described.[36] The compound **I** intermediates of the wild type and the W191G mutant CcP samples used for the EPR measurements were prepared by manually mixing directly in the 4-mm EPR tubes kept at 0 °C 2.5 mM native enzyme (100 mM potassium phosphate buffer, pH = 6.0) with equimolar/equivolume hydrogen peroxide. The reaction was stopped by rapid immersion of the EPR tube in liquid nitrogen, the overall procedure taking 15 s. For some of the experiments, the mixing time was increased up to 2 h by further incubation of compound **I** samples in ice (see Results). Stock solutions of hydrogen peroxide were prepared by dilution of 30% (v/v) H_2O_2 (Aldrich) in phosphate buffer. The concentration was determined by absorbance measurements at 240 nm ($\epsilon = 39.4\ M^{-1}\ cm^{-1}$).[37]

Generation of the In Vitro Tyrosyl Radical. Single crystals of tyrosine−HCl were obtained by slow evaporation, at room temperature, of L-tyrosine (Sigma) dissolved in a 30% solution of hydrochloric acid.

(17) In the case of CcP, the catalytically active intermediate has been referred to as compound ES to differentiate the protein-based radical in CcP from the porphyrin-based radical in horseradish peroxidase.

(18) Dunford, B. H. *Heme Peroxidases*; John Willey & Sons: New York, 1999.
(19) Housseman, A. L.; Doan, P.; Goodin, D. B.; Hoffman, B. M. *Biochemistry* **1993**, *32*, 4430−4443.
(20) Huyett, J. E.; Doan, P. E.; Gurbiel, R.; Houseman, A. L. P.; Sivaraja, M.; Goodin, D. B., Hoffman, B. M. *J. Am. Chem. Soc.* **1995**, *117*, 9033−9041.
(21) Benecky, M. J.; Frew, J. E.; Scowen, N.; Jones, P.; Hoffman, B. *Biochemistry* **1993**, *32*, 11929−11933.
(22) Hirst, J.; Wilcox, S. K.; Ai, J.; Jingyuan, A.; Moenne-Loccoz, P.; Loehr, T.; Goodin, D. B. *Biochemistry* **2001**, *40*, 1274−1283.
(23) Hisrt, J.; Wilcox, S. K.: Williams, P. A.; Blankenship, J.; Duncan, E.; McRee, D.; Goodin, D. B. *Biochemistry* **2001**, *40*, 1265−1273.
(24) Ivancich, A.; Jouve, H. M.; Sartor, B.; Gaillard, J. *Biochemistry* **1997**, *36*, 9356−9364.
(25) Ivancich, A.; Jouve, H. M.; Gaillard, J. *J. Am. Chem. Soc.* **1996**, *118*, 12852−12853.
(26) Khindaria, A.; Aust, S. D. *Biochemistry* **1996**, *35*, 13107−13111.
(27) Tsai, A.; Wu, G.; Palmer, G.; Bambai, B.; Koehn, J. A.; Marshall, P. J.; Kulmacz, R. *J. Biol. Chem.* **1999**, *274*, 21695−21700.
(28) Shi, W.; Hoganson, C. W.; Espe, M.; Bender, C. J.; Babcock, G. T. *Biochemistry* **2000**, *39*, 4112−4121.
(29) (a) Un, S.; Atta, M.; Fontecave, M.; Rutherford, A. W. *J. Am. Chem. Soc.* **1995**, *117*, 10713−10719. (b) Un, S.; Gerez, C.; Elleingand, E.; Fontecave, M. *J. Am. Chem. Soc.* **2001**, *123*, 3048−3054.
(30) Un, S.; Tang, X.-S.; Diner, B. A. *Biochemistry* **1996**, *35*, 679−684.
(31) Ivancich, A.; Mattioli, T. A.; Un, S. *J. Am. Chem. Soc.* **1999**, *121*, 5743−5753.
(32) Gerfen, G. J.; Bellew, B. F.; Un, S.; Bollinger, J. M.; Stubbe, J.; Griffin, R. G.; Singel, D. J. *J. Am. Chem. Soc.* **1993**, *115*, 6420−6421.
(33) Fournel, A.; Gambarelli, S.; Guigliarelli, B.; More, C.; Asso, M.; Choteau, G.; Hille, R.; Bertrand, P. *J. Chem. Phys.* **1998**, *109*, 10905−10913.
(34) Dorlet, P.; Boussac, A.; Rutherford, A. W.; Un, S. *J. Phys. Chem. B* **1999**, *103*, 10945−10954.
(35) Goodin, D. B.; McRee, D. E. *Biochemistry* **1993**, *32*, 3313−3324.
(36) Fitzgerald, M. M.; Churchill, M. J.; McRee, D. E.; Goodin, D. B. *Biochemistry* **1994**, *33*, 3807−3818.
(37) Nelson, D. P.; Kiesow, L. A. *Anal. Biochem.* **1972,** *49*, 474−478.

The crystals were irradiated with the γ-rays of a cobalt-60 source using a dose of 7 kGy/hr for 1 h at room temperature. Samples for HF-EPR measurements were prepared by finely grinding the crystals and homogenizing them in mineral oil. Samples were frozen in liquid N_2 for further use.

EPR Spectroscopy. The high-field EPR spectrometer has been described elsewhere.[31] The absolute error in *g*-values was 1×10^{-4}. The relative error in *g*-values between any two points of a given spectrum was 5×10^{-5}. Conventional 9 GHz EPR measurements were performed using a Bruker ER 200 spectrometer with a standard TE_{102} cavity equipped with a liquid helium cryostat (Oxford Instrument), a microwave-frequency counter (Hewlett-Packard 5350B) and NMR gaussmeter (Bruker ER035M).

Simulations of Exchange-Coupled Systems. Calculations were based on the Hamiltonian given in the theory section. Preliminary simulations to obtain an estimation of the coupling parameters were carried out by using the effective *g*-values that were obtained by perturbation theory (see theory section). In this case, variable parameters were estimated by nonlinear minimization of the root-mean-square difference between the calculated and experimental spectra using a standard conjugate gradient method.[38] Full calculations were processed by incrementing the magnetic field value. For each field value, the Hamiltonian matrix was calculated and numerically diagonalized to obtain the eigenvalues and eigenvectors. Transition probabilities among all possible combinations of levels were calculated and summed. The powder spectra were obtained by calculating the resonance for 10^6 random orientations of the applied magnetic field with respect to the *g*-axes system. The resulting orientation-integrated spectrum was convoluted with a derivative Gaussian line shape having a suitable line width. In the case of the full calculation, the simulated spectra were manually scaled to the experimental data. Gaussian distributions were obtained by the method of normal deviates.[38] All of the calculations were performed on a Digital Equipment Corporation workstation by using local programs written in Fortran 77.

Simulations of the Tyrosyl Radical Spectra. The simulations of the HF-EPR powder spectra of tyrosyl radicals were simulated by using locally written Fortran programs with standard numerical routines.[39] Distribution in *g*-values were simulated by introducing a tensor, the principal axes of which were collinear with the **g**-tensor. The principal values of the broadening tensor were the widths of Gaussian distributions along three directions.

Theory. The Hamiltonian that describes the interacting system of a spin $\mathbf{S} = 1$ ($\mathbf{S}^{Fe}$) with a spin $\mathbf{S} = 1/2$ ($\mathbf{S}^{rad}$) is given by

$$\mathbf{H} = \beta\, \mathbf{S}^{rad}\cdot\mathbf{g}^{rad}\cdot\mathbf{H} + \beta\, \mathbf{S}^{Fe}\cdot\mathbf{g}^{Fe}\cdot\mathbf{H} + \mathbf{S}^{Fe}\cdot\mathbf{D}\cdot\mathbf{S}^{Fe} + \mathbf{S}^{rad}\cdot\mathbf{\Delta}\cdot\mathbf{S}^{Fe}$$

where β is the Bohr magneton; **H,** the applied magnetic field; $\mathbf{g}^{rad}$ and $\mathbf{g}^{Fe}$ are the **g**-tensors for the radical and the iron center; **D** is the zero-field splitting tensor for the iron and is assumed to be axial; $\mathbf{\Delta}$ is the interaction tensor; and $\mathbf{S}^{rad}$ and $\mathbf{S}^{Fe}$, the spin operators. The tensors were assumed to be diagonal and collinear. The *z* direction is taken along the axis of symmetry of the zero-field splitting. Furthermore, we assume that $\mathbf{\Delta}$ is diagonal. With this assumption, the Hamiltonian can be expanded as follows in the system of axis chosen.

$$\begin{aligned}\mathbf{H} = \beta(g_x^{rad}\hat{S}_x^{rad}H_x + g_y^{rad}\hat{S}_y^{rad}H_y + g_z^{rad}\hat{S}_z^{rad}H_z + g_x^{Fe}\hat{S}_x^{Fe}H_x + \\ g_y^{Fe}\hat{S}_y^{Fe}H_y + g_z^{Fe}\hat{S}_z^{Fe}H_z) + D\left(\hat{S}_z^{Fe}\hat{S}_z^{Fe} - \frac{2}{3}\right) + \\ \Delta_x(\hat{S}_x^{rad}\hat{S}_x^{Fe}) + \Delta_y(\hat{S}_y^{rad}\hat{S}_y^{Fe}) + \Delta_z(\hat{S}_z^{rad}\hat{S}_z^{Fe}) \quad (1)\end{aligned}$$

The interaction between the iron center and the radical results in six energy levels. Because the values for the coupling are small compared to the positive zero-field splitting parameter D, the EPR spectra arise predominantly from transitions between the two lower levels. These levels result from the coupling of the $m_S = 0$ level of the iron with the $m_S = +1/2$ and $m_S = -1/2$ levels of the radical.[19] Perturbation theory can be used to show that the resulting spectrum for the coupled species can be described as a powder pattern with effective *g*-values depending on the interaction and zero-field splitting parameters. The Hamiltonian is split into H° and a perturbating term as follows:

$$\hat{H}^0 = \beta(g_x^{rad}H_xS_x^{rad} + g_y^{rad}H_yS_y^{rad} + g_z^{rad}\hat{S}_z^{rad}) + \beta g_z^{Fe}H_z\hat{S}_z^{Fe} + D\left(\hat{S}_z^{Fe^2} - \frac{2}{3}\right)$$

$$\hat{H}^p = \beta(g_x^{Fe}H_xS_x^{Fe} + g_y^{Fe}H_yS_y^{Fe}) + \Delta_xS_x^{Fe}\hat{S}_x^{rad} + \Delta_yS_y^{Fe}\hat{S}_y^{rad} + \Delta_zS_z^{Fe}\hat{S}_z^{rad}$$

We consider only the energy levels which implicate the $m_S = 0$ manifold of the metal center.

When the magnetic field is applied along the *x* direction, the energies to the second order of the two levels of interest are

$$E_1 = \frac{1}{2}\beta g_x^{rad}H_x - \frac{2}{3}D - \frac{1}{D}\left(\beta g_x^{Fe}H_x + \frac{\Delta_x}{2}\right)^2 + \frac{\Delta_y^2}{4}\frac{1}{\beta g_x^{rad}H_x - D}$$

$$E_2 = \frac{1}{2}\beta g_x^{rad}H_x - \frac{2}{3}D - \frac{1}{D}\left(\beta g_x^{Fe}H_x + \frac{\Delta_x}{2}\right)^2 + \frac{\Delta_y^2}{4}\frac{1}{\beta g_x^{rad}H_x + D}$$

and therefore,

$$h\nu = E_1 - E_2 = \beta g_x^{eff}H_x = \beta g_x^{rad}H_x - \frac{1}{D}(2\beta g_x^{Fe}H_x\Delta_x) + \frac{\Delta_y^2}{2}\frac{\beta g_x^{rad}H_x}{(\beta g_x^{rad}H_x)^2 - D^2}$$

In the case for which the Zeeman energy is small, as compared to the zero-field splitting, it follows that

$$g_x^{eff} = g_x^{rad} - 2g_x^{Fe}\frac{\Delta_x}{D} - \frac{1}{2}g_x^{rad}\frac{\Delta_y^2}{D^2} \quad (2)$$

In the same way, when the field is applied along the *y* direction, we have

$$g_y^{eff} = g_y^{rad} - 2g_y^{Fe}\frac{\Delta_y}{D} - \frac{1}{2}g_y^{rad}\frac{\Delta_y^2}{D^2} \quad (3)$$

When the magnetic field is applied along the *z* direction, the energies to second order are

$$E_1 = \frac{1}{2}\beta g_z^{rad}H_z - \frac{2}{3}D + \frac{(\Delta_x + \Delta_y)^2}{8}\frac{1}{\beta(g_z^{rad} - g_z^{Fe})H_z - D} + \frac{(\Delta_x - \Delta_y)^2}{8}\frac{1}{\beta(g_z^{rad} + g_z^{Fe})H_z - D}$$

$$E_2 = -\frac{1}{2}\beta g_z^{rad}H_z - \frac{2}{3}D + \frac{(\Delta_x + \Delta_y)^2}{8}\frac{1}{\beta(-g_z^{rad} + g_z^{Fe})H_z - D} + \frac{(\Delta_x - \Delta_y)^2}{8}\frac{1}{\beta(g_z^{rad} + g_z^{Fe})H_z + D}$$

therefore,

$$h\nu = E_1 - E_2 = \beta g_z^{eff}H_z$$

$$= \beta g_z^{rad}H_z - \frac{(\Delta_x - \Delta_y)^2}{4}\frac{(g_z^{rad} + g_z^{Fe})\beta H_z}{[(g_z^{rad} + g_z^{Fe})\beta H_z]^2 - D^2} + \frac{(\Delta_x + \Delta_y)^2}{4}\frac{(g_z^{rad} - g_z^{Fe})\beta H_z}{[(g_z^{rad} - g_z^{Fe})\beta H_z]^2 - D^2}$$

(38) Press, W. H.; Flannery, B. P.; Teukolsky, S. A.; Vetterling, W. T. *Numerical Recipes*; Cambridge University Press: New York, 1986.

(39) Dorlet, P.; Rutherford, A. W.; Un, S. *Biochemistry* **2000**, *39*, 7826−7834.

When the Zeeman term is small, as compared to the zero-field splitting, we have

$$g_z^{\text{eff}} = g_z^{\text{rad}} - (g_z^{\text{rad}} + g_z^{\text{Fe}})\left(\frac{\Delta_x - \Delta_y}{2\text{D}}\right)^2 - (g_z^{\text{rad}} - g_z^{\text{Fe}})\left(\frac{\Delta_x - \Delta_y}{2\text{D}}\right)^2 \quad (4)$$

As can be seen from the equations giving the effective *g*-values, the EPR spectrum for the coupled species is independent of Δ_z. Calculations based on the full diagonalization of the Hamiltonian verified the absence of Δ_z dependence for the oxoferryl iron−tryptophanyl radical system. Therefore, only Δ_x and Δ_y can be determined from the experimental data, and the component of the interaction tensor along the zero-field splitting axis remains undetermined. A second observation is that the effective *g*-values depend on the ratio Δ_i/D scaled by the *g*-values of the iron. In our simulations, the *g*-values for the radical and the iron were fixed to values reported in the literature.[40,19] The values obtained for the interaction parameters Δ_x and Δ_y are, therefore, relative to these values. For high magnetic fields, it is not possible to obtain the simple effective *g*-value expressions given in eqs 2−4, because the Zeeman terms are only modestly smaller than the parameter D in the case we study here. Hence, we expect a small but nonnegligible dependence on the magnetic field that can be used to further constrain the simulations.

Results

Multifrequency EPR Spectrum of the [(Fe(IV)═O) Trp$^{\bullet+}$] Intermediate of Wild-Type Cytochrome *c* Peroxidase: Spectral Simulations. Figure 1 shows the 10 K EPR spectra of the compound **I** intermediate of wild-type cytochrome *c* peroxidase that were obtained at four different frequencies (9.5, 95, 190, and 285 GHz). The compound **I** sample, used to record all four of the spectra, was obtained in 15s by the two-electron reaction of the high-spin ferric [Fe(III)] enzyme with hydrogen peroxide. Compound **I** has been previously assigned to a tryptophanyl radical in weak exchange interaction with the oxoferryl moiety.[11−14,19] The 9 GHz EPR spectrum has been previously modeled by an axial **g**-tensor, with effective values of $g_\perp \cong 2.01$ and $g_{||} \cong 2.04$, which results from a distributed exchange interaction (*J*).[19] The broadening of the 9-GHz spectrum (Figure 1, bottom), as compared to those recorded at higher frequencies, is due to hyperfine couplings; however, at higher frequencies, the *g*-anisotropy dominates over the hyperfine couplings. The spectra taken at the four different frequencies scaled roughly with frequency. Small frequency shifts of the g_x^{eff} and g_y^{eff} values were observed. g_x^{eff} shifted by about -1×10^{-2} from 95 to 285 GHz, and g_x^{eff}, by about -2×10^{-3}.

We have simulated the compound **I** CcP spectra using the Hamiltonian given by eq 1 in the Theory Section. The parameter D has been estimated to be ∼660 GHz.[9] This value was fixed in the simulations. From pertubation analyses discussed above (see Theory Section), the effective *g*-values clearly depend on the ratio of the spin-coupling value to D. Therefore, the coupling values determined from the simulations were only unique for a given D value. The *z* axis corresponds to the zero-field splitting symmetry axis. Because of this axial symmetry, the choice of the directions *x* and *y* is free. These axes are chosen by inspection of the crystallographic structure.[47a,b] The plane of the indole ring for Trp191 is almost perpendicular to the heme plane. The g_x direction of the organic radical, which, from theoretical considerations[41a,b,c] is assumed to go through the nitrogen atom of the ring, is parallel to the heme plane. Therefore, the *x* axis is chosen to coincide with the g_x direction of the radical and the *y* axis, to coincide with the g_z direction of the radical (indole ring perpendicular). The *z* axis matches, in good approximation, the g_y direction for the radical. In the (*x*, *y*, *z*) axis system, the *g*-values for the oxoferryl moiety are $g_x = g_y = 2.25$ and $g_z = 1.98$.[9] For the tryptophanyl radical, the *g*-values determined by high-field (35 GHz) EPR[30] are g_x=2.0033, g_y=2.0024, and g_z=2.0021 (F. Lendzian, private communication). Therefore, in the system of axes chosen, we have $g_x = 2.0033$, $g_y = 2.0021$, and $g_z = 2.0024$. The intrinsic *g*-values of the radical and the iron were fixed in the simulations.

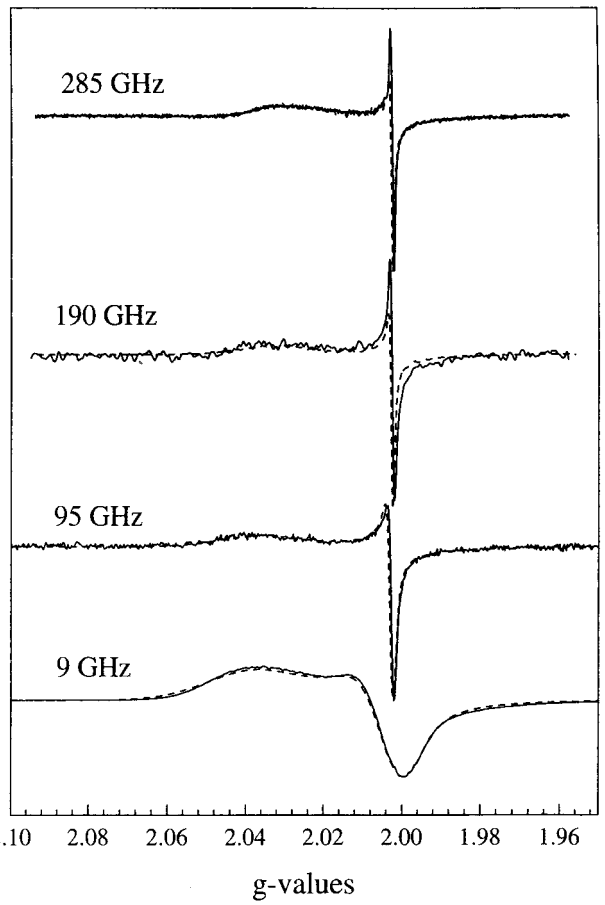

Figure 1. Multifrequency EPR spectra of the compound **I** intermediate [(Fe(IV)═O) Trp$^{\bullet+}$] of wild-type cytochrome *c* peroxidase. Spectra (1 scan) were recorded at 4 K and with a field modulation of 20 G. The simulated spectrum (dotted lines) is shown, together with the experimental spectrum for each frequency.

The simulated spectra are shown in Figure 1 (dotted lines), together with the experimental data. The simulations accurately reproduce the frequency-dependent shifts of the effective *g*-values. To reproduce the large width of the g_x^{eff} edge, as well as the high field tail of the signal (which results from the breadth

(40) Bleifuss, G.; Potsch, S.; Hofbauer, W.; Graslund, A.; Lubitz, W.; Lassman, G.; Lendzian, F. **1998**, In *Magnetic Resonance and Related Phenomena*, Proceedings of the AMPERE-ISMAR International Conference, Vol. II, 879−880.

(41) (a) Stone, A. J. *Proc. R. Soc. London, Ser. A* **1963**, *271*, 424−434. (b) Stone, A. J. *Mol. Phys.* **1963**, *6*, 509−515. (c) Stone, A. J. *Mol. Phys.* **1964**, *7*, 311−316.

(42) Hori, H.; Yonetani, T. *J. Biol. Chem.* **1985**, *260*, 349−355.

(43) Goodin, D. B.; Mauk, G.; Smith, M. *J. Biol. Chem.* **1987**, *262*, 7719−7724.

(44) Fishel, L. A.; Farnum, M. F.; Mauro, J. M.; Miller, M. A.; Kraut, J. *Biochemistry* **1991**, *30*, 1986−1996.

(45) It has been shown that the compound **I** intermediate has a $t_{1/2}$ of 6.6 ± 1.4 h (Erman &Yonetani, 1975).

(46) (a) Fasanella, E. L.; Gordy, W. *Proc. Natl. Acad. Sci. U.S.A.* **1969**, *62*, 299−304. (b) Liming, F. G.; Gordy, W. *Proc. Natl. Acad. Sci. U.S.A.* **1968**, 794−780. (c) Mezzetti, A.; Maniero, A. L.; Brustolon, M.; Giacometti, G.; Brunel, L.-C. *J. Phys. Chem. A* **1999**, *103*, 9636−9643.

(47) (a) Finzel, B. C.; Poulos, T. L.; Kraut, J. *J. Biol. Chem.* **1984**, *259*, 13027−13036. (b) Edwards, S. L.; Xuong, N.; Hamlin, R. C.; Kraut, J. *Biochemistry* **1987**, *26*, 1503−1511.

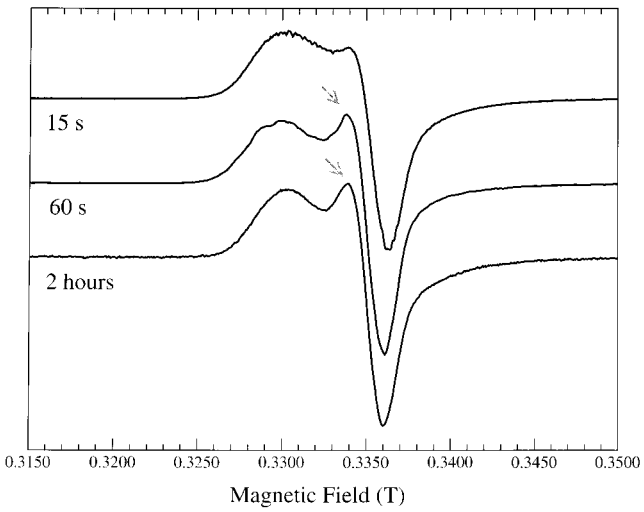

Figure 2. The 9-GHz EPR spectra of the [(Fe(IV)═O) $Trp^{\bullet+}$] intermediate of wild-type cytochrome *c* peroxidase obtained at different mixing times. The arrows indicate the minor differences between the spectra. Experimental conditions: temp, 4 K; microwave frequency, 9.437 GHz; modulation amplitude, 5 G; modulation frequency, 100 kHz; microwave power, 2 mW.

of the g_y^{eff} peak), it was necessary to use a distribution about the values of Δ_x and Δ_y, as already pointed out by Houseman and co-workers.[19] We modeled these distributions with Gaussian functions centered on Δ_i and with a half-width at half-maximum of σ_i. The parameters obtained for the interaction are $\Delta_x = -4.9$ GHz with a distribution $\sigma_x = 1.5$ GHz and $\Delta_y = -0.5$ GHz with a distribution $\sigma_y = 3.5$ GHz. A larger distribution for Δ_y, as compared to Δ_x, was required in order to properly fit the high-field tail of the EPR spectrum, as well as the relative amplitude ratio of the main features of the spectrum.

High-Field (285 GHz) EPR Spectrum of the [(Fe(IV)═O) $Trp^{\bullet+}$] Intermediate in Wild-Type Cytochrome *c* Peroxidase. Three different compound **I** samples were obtained by mixing at 0 °C wild-type enzyme with equimolar hydrogen peroxide for 15 s, 60 s, and 2 h before freezing. The 9-GHz EPR spectra of the three wild-type compound **I** samples confirmed that the ferric heme iron of the native enzyme was fully oxidized for all three of the different mixing times (data not shown). The $g \approx 2$ region of the 9-GHz EPR spectra showed the [(Fe(IV)═O) $Trp^{\bullet+}$] signal that was previously reported (Figure 2). In such spectra, the only noticeable difference between the compound **I** samples obtained at mixing times of 15 s and 60 s was the extra intensity contributing to the higher field region of the 9-GHz spectrum (arrows, Figure 2). The existence of such a narrow radical signal superposed to that of the exchange-coupled tryptophanyl radical has been a controversial issue in previous studies of the compound **I** in wild-type CcP and most of its mutants.[42−44,19]

Figure 3 shows the 285-GHz EPR spectra, recorded at 4 K, of the compound **I** samples obtained at mixing times of 15 s (top), 60 s (middle) and 2 h (bottom). The three spectra showed the EPR signal assigned to the exchange-coupled tryptophanyl radical (see previous section). Comparison of the HF-EPR spectra of the sample prepared with reaction times of 15 s and 60 s (Figure 3, top and middle) clearly shows that when the mixing time was increased to 60 s, a new EPR signal was superposed to that of the exchange-coupled tryptophanyl radical. Interestingly, after a longer reaction time (2 h) of the WT CcP with hydrogen peroxide in ice, the new EPR signal decreased considerably (Figure 2, bottom), but the tryptophanyl radical signal remained substantially unchanged.[45]

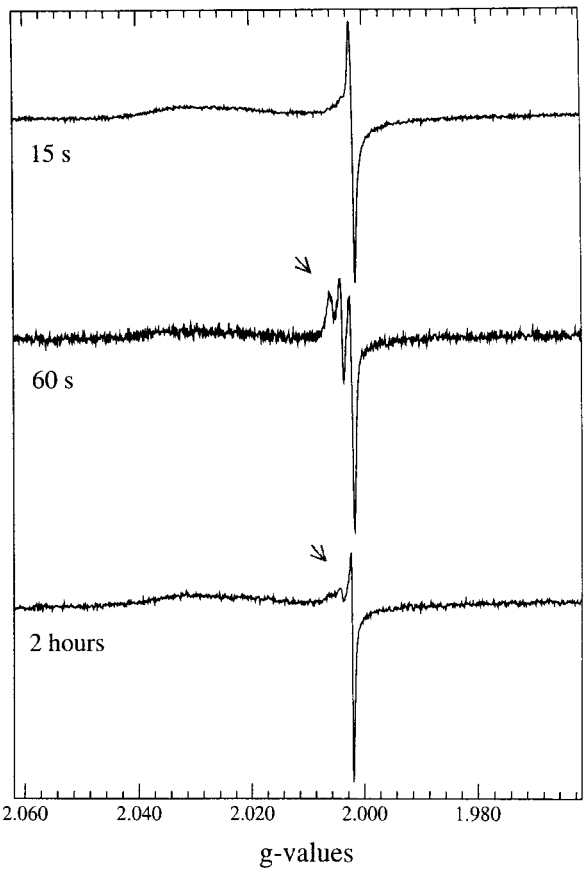

Figure 3. High-field (10 T, 285 GHz) EPR spectra of the [(Fe(IV)═O) $Trp^{\bullet+}$] intermediate of wild-type cytochrome *c* peroxidase obtained at different mixing times. The arrows indicate the presence of another radical species (see text). Spectra were recorded at 4 K using a field modulation of 20 G and a frequency modulation of 30 kHz.

Figure 4, bottom, shows the spectrum that was obtained by subtracting the HF-EPR spectra of the wild-type CcP compound **I** obtained at 60-s and 15-s mixing times. The difference spectrum corresponds to the short-lived radical species formed for a mixing time of 60 s. The powder-pattern spectrum showed three main field positions with observed *g*-values of 2.00644, 2.00436, and 2.00208. The difference spectrum was very similar to the neutral tyrosyl radical spectrum of bovine liver catalase, including the broad g_x-edge (Figure 4, bottom). The additional resonance in the difference spectrum, for which the observed *g*-value is 2.00282, was a subtraction artifact (asterisk, Figure 4).

Multifrequency EPR Spectra of the Compound I Intermediate in the W191G Mutant of Cytochrome *c* Peroxidase. The W191G compound **I** was obtained by the 15-s reaction of the mutant CcP with equimolar hydrogen peroxide. Figure 5 shows the 9-GHz EPR spectrum of the compound **I** intermediate of the mutant CcP recorded at 80 K. Such spectrum overlaps well with the tyrosyl radical ($Tyr^{\bullet}_{D}$) in Photosystem II (dotted lines). Thus, we assign the W191G compound **I** spectrum to a tyrosyl radical with the same proton hyperfine couplings as $Tyr_D^{\bullet}$ (Table 1). The power saturation study on the CcP radical gave a $P_{1/2}$ of 0.375 mW at 20 K, which is higher than that of the tyrosyl radicals in bovine liver catalase ($P_{1/2} = 0.060$ mW at 20 K) and PSII. Spin quantification of the radical signal yielded ~0.2 spins/heme.

HF-EPR was used to further characterize the radical intermediate formed in the W191G mutant CcP. Figure 6, middle, shows the HF-EPR spectra of the W191G compound **I** recorded

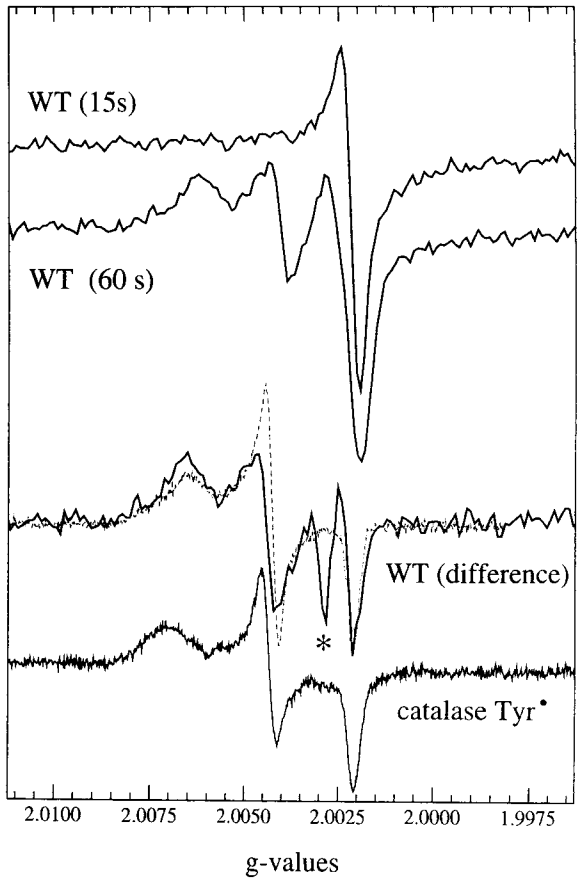

Figure 4. Expansion of the higher-field region of the [(Fe(IV)═O) $Trp^{\bullet+}$] intermediate spectra from Figure 3. The arithmetic difference between the 15-s and 60-s mixing time spectra (see text) is shown, together with the tyrosyl radical of bovine liver catalase.[31] The W191G compound **I** spectrum (gray dotted lines), recorded at 20 K and a field modulation of 5G, is superposed onto the difference spectrum.

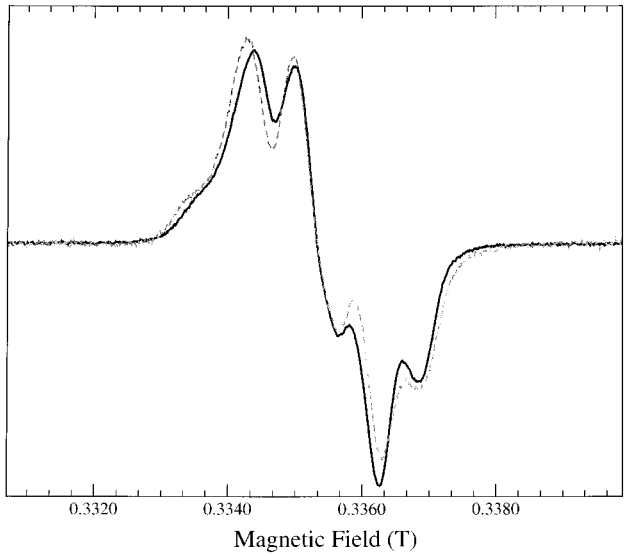

Figure 5. The 9-GHz EPR spectrum of the compound **I** intermediate of the W191G mutant cytochrome *c* peroxidase. The spectra of the tyrosyl radical in Photosystem II ($Tyr^{\bullet}_D$) is shown as a dotted line. Experimental conditions: temp, 80 K (10 K for $Tyr^{\bullet}_D$); microwave frequency, 9.441 GHz; modulation amplitude, 0.6 G (2.4 G for $Tyr^{\bullet}_D$); modulation frequency, 100 kHz; microwave power, 0.05 mW (2 mW for $Tyr^{\bullet}_D$).

at 190 and 285 GHz. The envelope of the HF-EPR spectrum is dominated by *g*-anisotropy, with resolved proton hyperfine

Table 1. Comparison of the **g** and Proton Hyperfine Coupling[a] Tensors of Compound **I** in the Mutant (W191G) Cytochrome *c* Peroxidase with the in Vitro and PSII Tyrosyl Radicals.

	in vitro $Tyr^{\bullet}_{HCl}$[d]	PSII $Tyr^{\bullet}_D$[b]	PSII $Tyr^{\bullet}_D$[c]	W191G CcP cpd I[d]
g_x	2.00658	2.00740	2.00756	2.00660
g_y	2.00404	2.00425	2.00432	2.00425
g_z	2.00208	2.00205	2.00215	2.00208
σ_x	0.00032		0.000036	0.00050
$H_{3,5}A_x$	−25.2	−25.4	−24.0	−24.0
A_y	−8.7	−7.2	−3.0	−3.0
A_z	−18.2	−19.5	−19.0	−19.0
$\phi_{3,5}$, deg	22	23	26	26
$H_{2,6}A_x$	5.0	4.48	5.0	5.0
A_y	5.0	7.28	5.0	5.0
A_z	5.0	4.48	5.0	5.0
$\phi_{2,6}$, deg	0	10	0	0
$H\beta_1 A_x$	39.2	20.2	31.0	31.0
A_y	39.2	29.3	28.0	28.0
A_z	39.2	20.2	27.0	27.0
$H\beta_2 A_x$	4.1	5.2	7.0	7.0
A_y	15.7	14.3	9.0	9.0
A_z	7.8	5.2	3.0	3.0

[a] MHz. [b] *Synechocystis* PSII: *g*-values from ref 30 and hyperfine couplings from refs 53, 54. [c] Spinach PSII from ref 39. [d] This work.

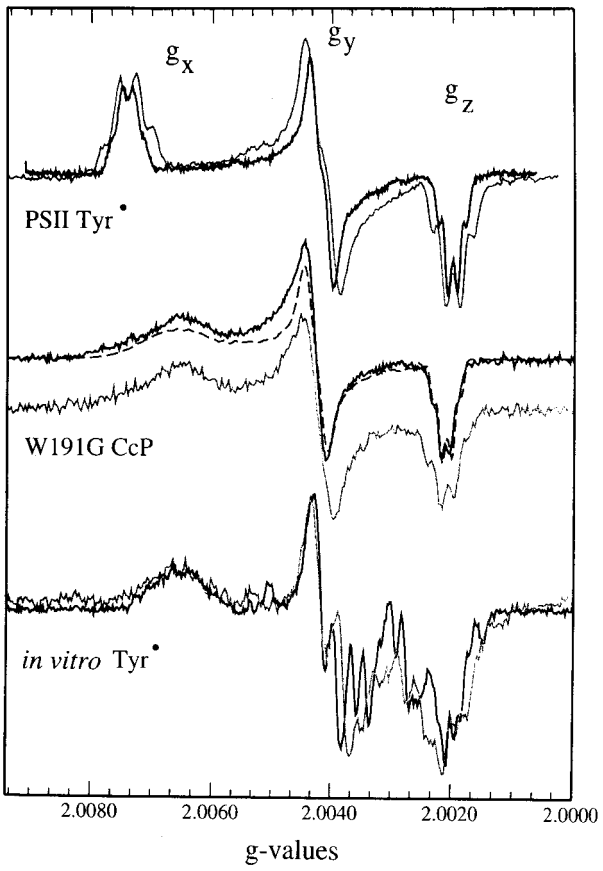

Figure 6. High-field 285 (solid black line) and 190 (solid gray line) GHz EPR spectra of the tyrosyl radicals in Photosystem II (top), the W191G mutant cytochrome *c* peroxidase (middle), and γ-irradiated Tyr-HCl crystals (bottom). The simulation of the 285 GHz spectrum of the CcP tyrosyl radical is superposed onto the experimental spectrum (dashed line). Spectra were recorded at 10 K, except for the CcP radical (20 K). In each case, the spectrum represents 1 scan and was obtained using a field modulation of 5 G (3 G for PSII).

coupling pattern mainly observed on the higher-field edge of the spectrum. The field positions of the three readily observed

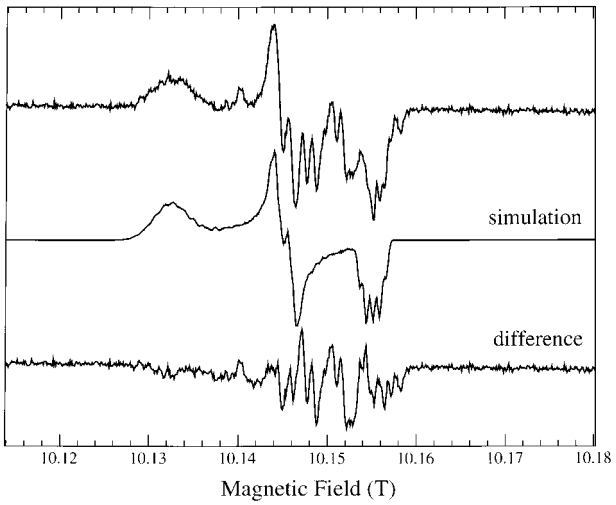

Figure 7. Experimental (top) and simulated (middle) high-field EPR spectrum of the in vitro tyrosyl radical obtained by γ irradiation of Tyr−HCl crystals. The spectrum (1 scan) was recorded at 10 K using a microwave frequency of 284.56 GHz and a field modulation of 5 G. The crystals were finely ground and homogenized in mineral oil to avoid orientation of the tyrosyl radical with the magnetic field.

features of the W191G compound **I** radical spectrum agree well with the principal *g*-values of other tyrosyl radicals (Figure 6). Specifically, the *g*-values of the compound **I** radical are almost identical to those of the in vitro tyrosyl radical (Table 1), including the broad g_x component (Figure 6, bottom). Comparison of the 285 and 190 GHz-EPR spectra of the W191G compound **I**, both plotted in *g*-values (Figure 6, middle), showed that the width of the g_x component is invariant and is the result of a distribution in *g*-values, which is similar to that of the in vitro $Tyr^{\bullet}$ (Figure 2, bottom). By contrast, the broadening observed for the g_z component at the lower microwave frequency was purely due to hyperfine couplings (spin−spin interactions), as for the PSII $Tyr^{\bullet}_{D}$ (Figure 6, top).

The powder pattern spectrum of the W191G compound **I** could be best simulated with *g*-values of 2.00660, 2.00425, and 2.00208 for g_x, g_y, and g_z respectively, and using the same hyperfine couplings of the PSII $Tyr^{\bullet}_{D}$ (see ref 39 and references therein). A distribution in g_x-values (with a Gaussian width of 0.0005) was needed to reproduce the broad low-field edge of the spectrum. The parameters used in the simulations are shown in Table 1, and the simulation is superposed to the experimental spectrum (dashed lines in Figure 6, middle).

High-Field EPR Spectrum of the In Vitro Tyrosyl Radical. Tyrosyl radicals can be obtained in vitro by γ-irradiation of tyrosine crystals. The HF-EPR spectrum, recorded at 285 and 190 GHz, of the in vitro tyrosyl radical ($Tyr^{\bullet}_{HCl}$) is shown in Figure 6, bottom. As expected, the powder spectrum was dominated by *g*-anisotropy with a resolved hyperfine pattern. The parameters used for the simulation of the HF-EPR spectrum (Figure 7, middle) are shown in Table 1. A distribution in g_x-values was needed to reproduce the broad low-field edge of the experimental spectrum. The HF-EPR spectrum showed that at least one other radical species was formed, together with the $Tyr^{\bullet}_{HCl}$. The EPR signal of such radical(s) mostly contributes at field positions between the g_y and g_z of the $Tyr^{\bullet}_{HCl}$ spectrum, as shown by the difference between the experimental and the simulated spectra (Figure 7, bottom). Longer exposures of the crystals to γ-irradiation gave a HF-EPR spectrum with an increasing proportion of other radical species relative to the $Tyr^{\bullet}_{HCl}$ (Supporting Information). The simultaneous formation of other radical species in the irradiated tyrosine crystals was not completely unexpected and has been reported previously.[46a,c] Although the original work on irradiated single crystals did not detect phenoxy-ring hydrogen addition products, they are known to occur in polycrystalline samples.[46a,b] Such species have a protonated phenoxy oxygen and lost aromaticity. The reduced *g*-anisotropy of the contaminating radical, as compared with the tyrosyl radical seen in the difference spectrum in Figure 7, is consistent with the loss of spin on the oxygen atom as a result of protonation.[29a] Even in the presence of the contaminating radical signal, it is possible to identify the likely g_y and g_z features of the $Tyr^{\bullet}_{HCl}$ on the basis of the relatively large library of HF-EPR spectra of tyrosyl radicals.[29−32] These features are much less sensitive to their environment.

Discussion

HF-EPR Spectrum of the (Fe(IV)═O) $Trp^{\bullet+}$) Intermediate in Wild-Type Cytochrome *c* Peroxidase. In contrast to a previous study,[19] we chose to model the interaction by a generalized spin-interaction Hamiltonian represented by a diagonal tensor, the principal axes of which are collinear with the **g**-tensors. Such interaction leads to a set of three effective *g*-values given by eqs 2−4. These expressions were rigorously expanded in terms of the different g_i and Δ_i (where *i* denotes the *x*, *y*, and *z* components) because of the higher resolution of high-field EPR with respect to *g*-anisotropy. However, it is clear that the spectra in Figure 1 cannot be characterized exactly by a single effective **g**-tensor. In contrast to the results predicted by perturbation theory, the turning points of the experimental spectra were field-dependent. A full Hamiltonian treatment was required to reproduce this behavior. Such an observation was made possible only by a multifrequency high-field EPR approach, where the effective *g*-anisotropy was dominant over the hyperfine interaction (Figure 1). In addition, as in the earlier work by Houseman,[19] distributions about the values Δ_x and Δ_y were required in order to properly fit the line shape of the EPR spectrum.

The description of the magnetic state for compound **I** by a weak interaction between the oxoferryl species and the tryptophanyl radical was first proposed by Houseman and co-workers (ref 19 and references therein). Their model was able to properly account for the apparently abnormal EPR signal observed for this state; however the values they obtained for the interaction components differ from ours. This is most likely the result of a difference in the modeling of the interaction. Houseman and co-workers have chosen to use a sum of isotropic exchange terms, $-J\mathbf{S}^{Fe}\cdot\mathbf{S}^{rad}$. In this representation, they obtained two contributions: two-third of the population exhibits an antiferromagnetic coupling centered at −1.45 GHz and with a distribution width of 1.2 GHz, and the remainder third of the population exhibits a ferromagnetic coupling centered at +2.9 GHz with a distribution width of 0.6 GHz. The authors note that the EPR spectra can be equally well-reproduced by a Heisenberg Hamiltonian with *J* described as a sum of three terms, as compared with the use of a spin-coupling tensor.[19]

The fundamental difference between the two models is that Houseman and co-workers assume a purely isotropic spin−spin interaction, whereas in the present work, an anisotropic interaction is used. The anisotropic model has two contributions, the isotropic component due to Heisenberg exchange and an anisotropic component due to dipolar coupling. In principle, it is possible to obtain the isotropic component of the anisotropic interaction by calculating the trace of the tensor; however, as discussed above, the spectra are to the second order independent of the *z* component of the spin-coupling tensor, and therefore,

Table 2. Environment of Candidates for the Tyrosyl Radical Site in the W191G Mutant Cytochrome *c* Peroxidase.

Tyr position	Tyr251	Tyr244	Tyr187	Tyr153	Tyr236
H_β dihedral angle, deg	67	66.4	3.7	0.7	82.5
O_{Tyr}−Fe dist, Å	16.7	14.0	11.6	11.8	18.9
H bond donor(s)	Asp261	water 328	waters 345, 346	none	none
H bond dist, Å	1.62	1.66	1.9, 2.3		
Lys residue	Lys257	Lys243	Lys149	Lys149	Lys
NH_{Lys}−O_{Tyr} dist, Å	4.3	7.5	7.0	5.5	13.0
Arg residue	Arg166	Arg155	none	Arg160	none
NH_{Arg}−O_{Tyr} dist, Å	3.8	4.3		7.0	

in general it is not possible to directly determine the trace. The fact that the component of the interaction along the *y* axis is essentially zero leads to the conclusion that the dipolar and exchange contributions exactly cancel along this direction. If we assume a point−dipole model, the dipole−dipole vector can be oriented in one of three possibilities (i.e., along *x*, *y*, or *z*). However, only the case in which the dipolar vector is along *x* yields parameters that are consistent with the values obtained for Δ_x and Δ_y as well as the necessary requirement that the dipole coupling coefficient ($\delta = \mu^0 g^{Fe} g^{rad} \beta^2 / 4\pi r^3$) be a positive value. This leads to $\Delta_x = J - 2\delta$ and $\Delta_y = J + \delta$, and values can therefore be calculated for *J* and δ. Using this approximation, the exchange coupling *J* is −2.3 GHz, which is comparable to the value obtained by Houseman and co-workers for the antiferromagnetic contribution (−1.45 GHz[19]). The dipole coupling value, 1.8 GHz, yields a spin−spin distance of 3.1 Å, which is inconsistent with the crystal structure[47a] (7.1 Å from iron to indole nitrogen).[48] The discrepancy is probably due to the inadequacy of the point−dipole approximation for calculating distances in such cases, rather than the assumption of collinearity of the dipole vector with the *g*-axis. The crystallographic structure suggests that the dipole vector is rotated in the *xz* plane of the **g**-tensor and is not collinear with either axis. Preliminary calculations using a rotated interaction tensor that is consistent with the structure did not yield better fits or significantly weaker couplings.

One way to distinguish between the purely isotropic and anisotropic models is to examine single-crystal data. For an anisotropic interaction, the EPR spectrum of a single crystal sample is predicted to be a single line. In contrast, when the coupling is a sum of two isotropic contributions, the EPR spectra is constituted by two lines; that is, each contribution gives rise to a single line. Indeed, only one component was found during the analysis of the single crystal data, but measurements done on a polycrystalline sample gave essentially the same results as in frozen solution.[19] This is fully consistent with a single interaction tensor and supports our modeling of the spin−coupling interaction, as compared to a sum of isotropic terms. In this regard, because the shifts of the *g*-values, $g_x^{eff} - g_x^{rad}$ and $g_y^{eff} - g_y^{rad}$, induced by the interaction are different, it follows that the interaction in this case must have anisotropic character. A single essentially isotropic interaction is unable to account for the observed experimental spectra.

Tyrosyl Radical Intermediate in W191G Cytochrome *c* Peroxidase. The HF-EPR spectrum of the in vitro tyrosyl radical confirmed the previously reported *g*-values.[46a] In particular, the low g_x-value (2.00658) can be directly correlated to an electrostatic effect (electropositive) of the environment on the tyrosyl radical.[29a,b] Additional information concerning the microenvironment of the $Tyr^{\bullet}_{HCl}$ was also obtained from the HF-EPR spectrum. The broad g_x-value is indicative of an inhomogeneous environment, similar to that of the tyrosyl radicals in Photosystem II ($Tyr^{\bullet}_Z$)[30] and bovine liver catalase[31] (Figure 4).

We have used high-field EPR to characterize the peroxide intermediate of the CcP mutant in which Trp191 was replaced by a glycine residue. The powder-pattern spectrum of the W191G compound **I** could be best simulated with the same *g*-values as those of the in vitro tyrosyl radical. In contrast, the hyperfine couplings (observed both at conventional and higher fields) were the same as those of $Tyr^{\bullet}_D$ in Photosystem II. From these observations, we conclude that the radical intermediate in the mutant CcP is a tyrosyl radical with the same **g**-tensor as the $Tyr^{\bullet}_{HCl}$ and proton-hyperfine coupling tensor as PSII $Tyr^{\bullet}_D$ (Table 1).

Taking into account the information regarding the electrostatic microenvironment of the tyrosyl radical obtained from the high-field EPR spectrum of the W191G compound **I**, we examined the three-dimensional structures of the 14 tyrosines in the mutant CcP.[36] Residues at positions 251, 244, 187, and 153 are good candidates for the radical site. Those tyrosines are on the proximal side and relatively close to the heme iron (<17 Å). The low g_x-value of the in vitro tyrosyl radical is due to the effect of an electropositive environment, specifically to the presence of a strong hydrogen bond at a distance of 1.60 Å, and donated by the protonated carboxylic group of a neighboring tyrosine.[49a] Presumably, a positively charged residue could yield the same g_x-value.[29b] The distances to possible hydrogen-bond donors and positively charged amino acid residues related to the tyrosine residues in W191G CcP are given in Table 1. The combined effect of hydrogen bond(s) donor(s) and positive charges in the microenvironment of tyrosines 251, 244, and 187 would explain the low g_x-value (with maximum at 2.00660) and the broadening (distribution of 0.0005) observed for the tyrosyl radical of W191G compound **I**. Interestingly, the strong hydrogen bond formed by the carboxyl group of Asp261 (1.62 Å) on Tyr251 would be equivalent in strength to that observed for the in vitro tyrosyl radical and would explain the almost identical *g*-values (Table 1). Alternatively, Tyr244 and Tyr187 are also interesting candidates because of the presence of structural water(s) at hydrogen-bonding distance(s) together with a close lysine. Finally, the dihedral angles (θ) related to the β-protons of tyrosines 251 and 244 obtained from the crystal structure[36] of the W191G mutant CcP are in good agreement with those estimated from the experimental hyperfine couplings.

In a previous study, Tyr236 was proposed as the radical site because of the covalent modification due to the reaction of the mutant CcP with hydrogen peroxide and 2-aminothiazole.[50] As shown in Table 2, Tyr236 is very isolated (no potential hydrogen bond donors or positively charged amino acid residues close by). Accordingly, the g_x-value of such a tyrosyl radical should be similar to that of the tyrosyl radical in ribonucleotide reductase[29] (2.00890) and, thus, inconsistent with that observed in this work (2.00660). The reaction of CcP with hydrogen peroxide and 2-aminothiazole was carried out at room temperature; thus, it is likely that the tyrosine residue previously identified (Tyr236)[50] became oxidized by intermolecular electron transfer from the compound **I** tyrosyl radical that was observed

(48) A similar situation has been encountered in the treatment of the coupling between the nonheme iron and a semiquinone radical in bacterial reaction centers in which the distance that is obtained from the anisotropic spin−spin interaction coupling is also underestimated by a factor of 3 (see Buter, W. F.; Calvo, R.; Fredkin, D. R.; Issacson, R. A.; Okamura, M. Y.; Feher, G. *Biophys. J.* **1984**, *45*, 947−973).

(49) Frey, M. N.; Koetzle, T. F.; Lehman, M. S.; Hamilton, W. C. *J. Chem. Phys.* **1973**, *58*, 2547−2556.

(50) Musah, R. A.; Goodin, D. B. *Biochemistry* **1997**, *36*, 11665−11674.

in this work. Further studies with mutants on these tyrosine residues could be helpful in discerning among the possible candidates for the radical site.

The "Narrow" EPR Signal in Wild-Type CcP Compound I. The observation of an additional "narrow" signal on the 9 GHz EPR spectrum of the compound **I** in wild-type CcP has been a controversial issue since the early report of Hori and Yonetani[42] on the single-crystal EPR studies performed at 3, 9, and 35 GHz. From such studies, the authors concluded that the narrow radical signal should originate from the oxidation of a protein residue that is different from the compound **I** radical species. Other authors also found an additional narrow radical signal in the 9 GHz EPR of compound **I** (frozen solution) present in lower concentrations (10−20%).[43,42,51] By contrast, relaxation measurements made by using pulsed EPR on the CcP compound **I** samples prepared by Hoffman and co-workers provided no evidence of an additional radical species.[19]

In all of these studies, the mixing time used to prepare the CcP compound **I** was not mentioned by the authors, with the exception of Fishel and co-workers.[44] In the latter, 1−1.5-fold excess of hydrogen peroxide was used to prepare the compound **I** samples using a mixing time of 1 min. For such experiments, the native enzyme concentration was 0.2−0.7 mM.[44] Hoffman and co-workers used native enzyme (about 1 mM) in 30−60% glycerol with 2−5-fold H_2O_2 excess, but the mixing time was not quoted.[19] These authors interpreted the presence of an additional narrow radical reported by Hori and Yonetani[42] or Goodin and co-workers[43] as the result of overoxidation in compound **I** samples that were not properly prepared or as a result of a subset of molecules for which the tryptophanyl radical was not magnetically coupled to the oxoferryl heme.

We have monitored the compound **I** formation by using HF-EPR and different mixing times. Our results show that the exchange-coupled tryptophanyl radical was readily formed within 15s and was stable for at least 2 h at 0 °C. Another radical species was formed when using a mixing time of 1 min; it almost disappeared when the sample was incubated for 2 h. The higher resolution of *g*-anisotropy obtained at higher fields allowed us to clearly resolve two different radicals by their *g*-values (Figure 3). The previous observations concerning the presence of a narrow radical (see, for example, ref 44) were based on subtle differences in the EPR spectra at conventional fields (Figure 2).

The controversial EPR results concerning the narrow radical species previously reported by the different groups, as well as the importance of the mixing dynamics (mixing time, sample concentration, viscosity, temperature) can be rationalize by our findings. Fishel and co-workers[44] observed the narrow radical species when spending 1 min to mix the native (WT) CcP with H_2O_2. Hoffman and co-workers, who did not specify the mixing time, used, in addition, 30 to 60% glycerol in their native CcP samples.[19] In the latter case, the glycerol made the native sample more viscous, thus changing the conditions of the reaction. Accordingly, the absence of the second radical species in such samples can be reasonably explained by the fact that the short-lived species had already vanished, as demonstrated by our experiments (Figure 3).

The HF-EPR spectrum of the short-lived radical in wild-type CcP is very similar to that of the tyrosyl radical observed for the W191G compound **I** (Figure 4). In both cases, they are formed in low concentration (10−20%). Moreover, the *g*-anisotropy (defined as $\Delta g = |g_x - g_y|$) of the short-lived radical is too large (0.0046) for that of an uncoupled tryptophanyl radical ($\Delta g = 0.0012$).[40] Thus, in agreement with previous suggestions, we propose that the short-lived species is a tyrosyl radical.[52] The essentially identical *g*-values and distribution in g_x-value that were obtained from the HF-EPR spectra of the tyrosyl radicals in wild-type and W191G mutant CcP (Figure 4) strongly suggests an equivalent electropositve environment for both of the radicals. Accordingly, the good candidates for the radical site found in both enzymes are the three tyrosines at positions 251, 244, and 187 (Table 2). Site-directed mutagenesis on such tyrosine residues or on their microenvironment combined with HF-EPR spectroscopy is a powerful approach to discern among these possibilities.

Acknowledgment. We thank Dr. A. William Rutherford for his support of this work and Dr. C. Roselli and Prof. C. Houée-Levin (Laboratoire de Physico-Chimie des Rayonnements, Université Paris Sud, Orsay) for the use of the cobalt-60 source and stimulating discussions. Financial support was provided by the European Union HCM Research Network (Contract no. FMRX-CT98-0214, to A.I.), the Human Frontiers Science Organization (Contract no. RGO349), Region Ile-de-France (Contract Sesame) and CEA-Saclay, and by Grant GM41049 from the National Institutes of Health (to D.B.G.).

Supporting Information Available: HF-EPR spectra of the in vitro tyrosyl radical obtained with longer exposure times. This material is available free of charge via the Internet at http://pubs.acs.org.

JA0036514

(51) Scholes, C. P.; Liu, Y.; Fishel, L. A.; Farnum, M. F.; Mauro, J. M.; Kraut, J. *Isr. J. Chem.* **1989**, *29*, 88−92.

(52) It is noteworthy that the HF-EPR spectrum of a tryptophanyl radical with very small *J* values could be virtually identical to that of a tyrosyl radical.

(53) Warncke, K.; Babcock, G. T.; McCracken, J. *J. Am. Chem. Soc.* **1994**, *116*, 7332−7340.

(54) Tommos, C.; Madsen, C.; Styring, S.; Vermass, W. *Biochemistry* **1994**, *33*, 11805−11813.